https://doi.org/10.5194/essd-2026-89
Preprint. Discussion started: 23 February 2026

Open Access Earth System Science Data Discussions

A global eddy-collocated temperature and salinity profile dataset (v1.0): integrating multiplatform *in situ* observations with satellite-detected mesoscale eddies

Qingyou He[1,2], Yunchen Liu[1,3], Weikang Zhan[1,2], Yinghui He[1], Zhenting Mo[1,3], Peiya Zhang[1,3], Shuqun Cai[1,3], and Haigang Zhan[1,2]*

[1]State Key Laboratory of Tropical Oceanography, South China Sea Institute of Oceanology, Chinese Academy of Sciences, Guangzhou, China

[2]Guangdong Key Lab of Ocean Remote Sensing and Big Data, South China Sea Institute of Oceanology, Chinese Academy of Sciences, Guangzhou, China

[3]University of Chinese Academy of Sciences, Beijing, China

*Corresponding author: Haigang Zhan (hgzhan@scsio.ac.cn)

Abstract

Mesoscale eddies are a fundamental component of ocean circulation and play a crucial role in shaping the three-dimensional distribution of ocean temperature and salinity. However, observational constraints have long limited systematic, global-scale quantification of eddy-induced thermohaline variability. Here, we present a global eddy-collocated historical temperature and salinity profile dataset spanning 29 years (1993–2021), constructed by integrating in situ hydrographic profile observations with satellite-derived mesoscale eddy tracking products. The dataset contains 2.35 million quality-controlled temperature-salinity profiles, each collocated with the nearest mesoscale eddy on the sampling day that may have influenced the observed water column. The profiles provide broad global coverage, with most 2°×2° grid boxes containing more than 150 observations, enabling statistically robust analyses from regional to global scales. Validation against well-documented regional eddy signatures shows that the dataset consistently reproduces well-established eddy-induced temperature and salinity anomaly structures across diverse ocean regions. Example applications demonstrate the dataset's capability to investigate the spatial heterogeneity and vertical extent of eddy-induced thermohaline anomalies, eddy impacts on mixed-layer depth and stratification, eddy contributions to subsurface extreme temperature events, and eddy-driven heat and material transports. This dataset provides a comprehensive observational foundation for advancing quantitative assessments of mesoscale eddy impacts on regional to global ocean physical environment, heat budgets, and climate change.

https://doi.org/10.5194/essd-2026-89
Preprint. Discussion started: 23 February 2026

Open Access Earth System Science Data Discussions

1. Introduction

Mesoscale eddies, as rotating currents with horizontal scales of *O*(100 km) and lifespans of weeks to months, are one of the most energetic and ubiquitous features in the global ocean (*Chelton et al.*, 2011b). These features occupy 25-30% of the global ocean surface and account for 90% of the total kinetic energy in the ocean (*Chaigneau et al.*, 2009; *Ferrari and Wunsch*, 2009). Through vertical thermohaline displacements, rotational advection, and lateral trapping (*Gaube et al.*, 2014; *McGillicuddy*, 2016), eddies generate pronounced temperature and salinity perturbations that can extend hundreds to even thousands of meters below the sea surface (*Frenger et al.*, 2015; *He et al.*, 2018; *Sun et al.*, 2017), playing essential roles in modulating upper-ocean heat distribution (*Dong et al.*, 2014; *He et al.*, 2024a; *Sun et al.*, 2019), regional circulation (*Jan et al.*, 2017; *Jing et al.*, 2020; *Zhang et al.*, 2014), biogeochemical environments (*Amos et al.*, 2019; *Arostegui et al.*, 2022; *He et al.*, 2021; *Omand et al.*, 2015), and marine animal behaviors (*Arostegui et al.*, 2022; *Braun et al.*, 2025; *Braun et al.*, 2019). These impacts highlight the importance of characterizing the three-dimensional thermohaline structure of eddies and quantifying their contributions to regional-to-global heat and freshwater redistributions.

Key scientific questions remain regarding the vertical structure, regional variability, and cumulative effects of eddy-induced thermohaline anomalies. For example, the intensity and penetration depths of eddy-associated temperature and salinity anomalies differ substantially across ocean basins (*Lin et al.*, 2015; *Schütte et al.*, 2016; *Yang et al.*, 2013; *Zhang et al.*, 2018), influenced by background stratification, eddy nonlinearity, life-cycle stage, and interactions with mean currents and topography (*He et al.*, 2020; *Liu et al.*, 2019; *Moreau et al.*, 2017; *Samelson et al.*, 2014). Quantifying eddy-driven temperature and salinity anomalies and the associated heat and freshwater transports thus require large-amount observations that are targeted to eddy fields.

Significant progress has been made over the past two decades with the development of high-resolution satellite altimetry products (e.g., the AVISO products) and automated eddy detection and tracking algorithms (*Chelton et al.*, 2011b). Although individual eddies vary in shapes, eddy-centric composite analyses reveals that the mean sea-level anomalies of eddies in a relatively small region exhibit a coherent monopole structure (*Gaube et al.*, 2013; *He et al.*, 2017), indicating that eddies have a robust regional mean character (*Zhang et al.*, 2013). By collocating altimetric eddy fields with other concurrent satellite observations, the composite analysis has been widely used to reveal regional mean eddy impacts on sea surface temperature (*Lv et al.*, 2022; *Ni et al.*, 2021; *Zhan et al.*, 2023), salinity (*Delcroix et al.*, 2019; *Hasson et al.*, 2019; *Trott et al.*, 2019), chlorophyll (*Chelton et al.*, 2011a; *Frenger et al.*, 2018; *He et al.*, 2021), and air-sea fluxes (*Frenger et al.*, 2013; *Guo and Timmermans*, 2024; *Villas Bôas et al.*, 2015).

Concurrently, *in situ* observing systems, such as mooring arrays, Argo floats, and gliders, have expanded rapidly. The World Ocean Database (WOD) now have collected millions of historical available temperature and salinity profile observation data from diverse instruments and platforms (*Boyer et al.*, 2016; *Riser et al.*, 2016), making regional to global eddy-profile collocation feasible. Studies using Argo profile data or subsets of WOD archives have demonstrated eddy-driven thermohaline anomalies and the associated transports in the South China Sea (*He et al.*, 2018; *Sun et al.*, 2018), the Indian Ocean (*de Marez et al.*, 2019; *Gulakaram et al.*, 2020; *Yang et al.*, 2015), the western Pacific (*Dong et al.*, 2017; *Sun et al.*, 2017), the Southern Ocean (*Frenger et al.*, 2015;

https://doi.org/10.5194/essd-2026-89
Preprint. Discussion started: 23 February 2026

Laxenaire et al., 2019), and globally (*Dong et al.*, 2014; *Sun et al.*, 2019). However, most of existing studies focus on specific regions, time periods, instrument types, or coarse statistic grids, limiting global comparability (*Wei and Wang*, 2025; *Xu et al.*, 2016; *Yang et al.*, 2013). Sampling biases arise because profiling observations do not uniformly sample eddy interiors or life-cycle stages (*Chaigneau et al.*, 2011). Methodological differences across studies, such as eddy detection algorithms, profile quality-control procedures, and eddy-profile collocating methods, also hinder synthesis (*Chaigneau et al.*, 2008; *He et al.*, 2018; *Liu et al.*, 2019; *Sun et al.*, 2018). Notably, there is no unified, quality-controlled, and radius-normalized global dataset that systematically matches the historical available temperature and salinity profiles with satellite-identified eddies throughout the altimetry era.

Here we address this gap by constructing a global eddy-collocated temperature and salinity profile dataset that integrates the world's most extensively accumulated historical profile dataset (form the-WOD) with mesoscale eddies identified from satellite altimetry (Fig.1). All profiles collected during the satellite altimetry period are matched to the nearest eddy realization, and the profile–eddy distance is normalized by the eddy radius to provide a consistent spatial framework for composite and process-oriented analyses. Validations against published Argo-based studies are processed to check the reliability of the data in capturing regional eddy thermohaline structures. Example applications are also provided to demonstrate the dataset's utility for characterizing regional and global eddy-induced thermohaline anomalies, mixed-layer perturbations, extreme temperature events, and eddy-driven transports. By combining the extensive historical coverage of the WOD data with the dynamical context of satellite altimetry, this unified dataset provides a reproducible foundation for advancing studies of the physical and thermohaline impacts of mesoscale eddies across the global ocean and supports relevant model evaluation, ocean state estimation, and climate change research.

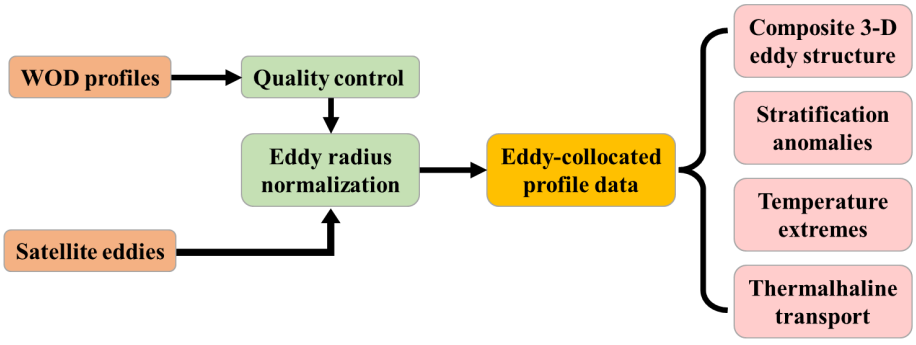

Fig.1 Flowchart illustrating the data source, main workflow, and potential implications of eddy-collocated profile dataset.

2. Data and methods

2.1 Mesoscale eddy product

Mesoscale eddies were identified and tracked based on overlapping closed contours of daily absolute dynamic topography (ADT) fields from multi-satellite altimeter data (Pegliasco et al., 2022). The global mesoscale eddy trajectory atlas product (META3.2, allsat) used in this study was produced by SSALTO/DUACS and distributed by AVISO^{+}. The eddy product contains daily time series of the

https://doi.org/10.5194/essd-2026-89
Preprint. Discussion started: 23 February 2026

position, polarity (cyclonic/anticyclonic), amplitude, radius, rotational speed, and associated edge contours of each identified and tracked eddy trajectory between January 1993 and February 2022. Only those eddies with lifetimes longer than 10 days were considered have stable structures and used in this study.

In the Northern Hemisphere, eddies with regional extreme low (high) sea level anomalies and rotate anticlockwise (clockwise) are defined as cyclonic eddies (anticyclonic eddies). The vice versa in the Southern Hemisphere. Eddy radius is estimated as the radius of the best fit circle corresponding to the contour of maximum circum-average geostrophic speed at eddy edge (Pegliasco et al., 2022). Eddy amplitude is defined as the absolute SSH difference between the extremum sea level anomaly in eddy center and that at edge. Eddy rotational speed is estimated as the average geostrophic speed of the contour defining the speed radius. Eddy edge contour is the contour of maximum circum-average geostrophic speed for the detected eddy. A detailed description of the process of eddy detection, eddy tracking and the statistics of eddy outputs can be found in Pegliasco et al. (2022). Based on eddy edge contours, we estimated eddy occurrence probability, at each 1/4°×1/4° grid point, as the percentage of days a point is located within eddy interiors during the observation period.

2.2 Historical temperature and salinity profiles

The World Ocean Database (WOD) collected global historical available temperature and salinity profile measurements since Captain Cook's 1772 voyage from a wide range of instruments and platforms, including ocean station data (OSD), ship-based conductivity–temperature–depth (CTD), expendable bathy thermograph (XBT), Argo float, moored buoy, drifter buoy, Autonomous Pinniped data (APB), glider and others (Boyer et al., 2016). These profile measurements constitute the most comprehensive global *in situ* observation dataset, providing invaluable support for investigating ocean environment states and their changes under global warming. In this work, we extracted temperature and salinity profiles with quality control flags marked as '0' (accepted) during the period of satellite altimetry–derived eddy observations (January 1993 and December 2021).

2.3 Quality control process

In addition to the quality control carried out by the WOD, we additionally excluded profiles that (1) lacked measurements shallower than 20 m or deeper than 200 m, (2) contained fewer than 10 unique samples within the upper 200 m, or (3) exhibited vertical sampling intervals larger than 15 m between 0–100 m or larger than 25 m between 100–200 m (He et al., 2020). These criteria remove profiles with coarse vertical resolutions that would otherwise introduce errors when they were interpolated to normalized high-resolution vertical grids, particularly across thermocline layers with strong vertical gradients. Then, all the remained profiles were vertically interpolated onto a uniform grid from 0 to 2,000 m depth, with vertical intervals of 5 m between 0-1,000 m, 10 m between 1,000-1,500m, and 50 m between1,500-2,000 m.

2.4 Collocating profile observations to eddy fields

To collocate in situ profile measurements to mesoscale eddies, we assumed that a given profile is influenced primarily by the eddy closest to its sampling location. For each profile, we searched for the nearest eddy (either cyclonic eddy or anticyclonic eddy) on the same sampling day and collocated the two. As eddies vary in size and shape, the distance between the profile and the collocated eddy's center was normalized by eddy radius, i.e., the distance between eddy center and eddy edge in the same

https://doi.org/10.5194/essd-2026-89
Preprint. Discussion started: 23 February 2026

direction of the profile (Fig.2). This normalization favors the comparison of eddies of different shapes and sizes and enables a consistent dimensionless composite analyses of eddies' thermal and biogeochemical imprints.

This profile-collocating approach differs from methods that search for profiles around each eddy realization (*Chaigneau et al.*, 2011; *Sun et al.*, 2017; *Yang et al.*, 2015). Considering that satellite altimetry typically resolves many more eddies than the ocean is sampled by in situ profilers (especially before 2010), associating profiles with their closest eddy is computationally efficient and avoids double counting. It also prevents a single profile from being simultaneously assigned to both the interior of one eddy and the periphery of another, an ambiguity present in "search-eddy-surrounding" methods, particularly when eddies cluster.

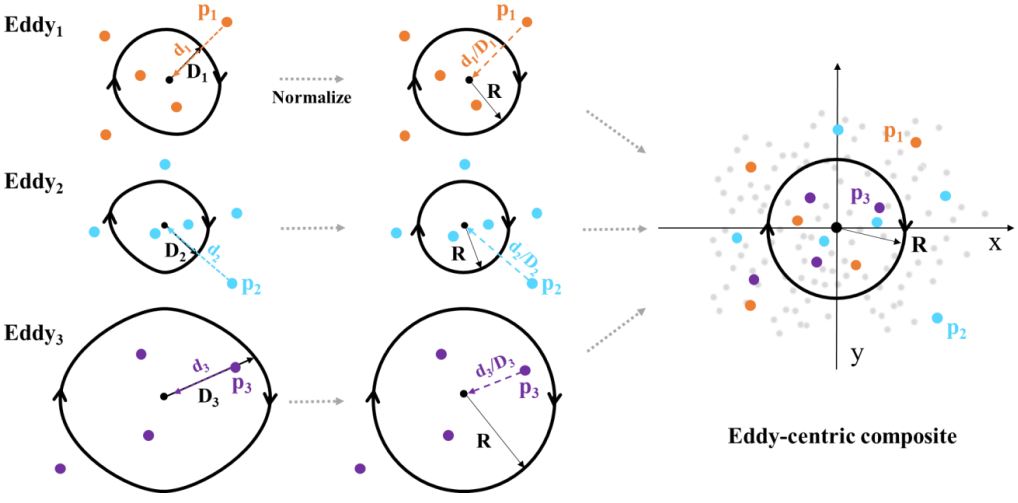

Fig.2 Schematic demonstrating the process of collocating WOD profiles to the nearest eddy and compositing them to a radius-normalized eddy-centric coordinate. The circles are eddies of various sizes and the dots are data profiles.

2.5 Eddy imprints extraction

As the profiles were near randomly sampled around or within different locations of different eddies, we cannot obtain the three-dimensional structure of a specific eddy. Whereas, within a relatively small region with relatively uniform thermal and dynamical environments, eddies are expected to share some common characteristics. Thus, we can reveal the mean eddy structure by compositing eddy-associated observations to a uniform radius-normalized eddy-centric coordinate system (Fig.3). To isolate eddy-associate temperature/salinity anomalies, each profile measurement was subtracted by the corresponding climatological monthly mean value at the closest matching point, from the World Ocean Atlas 2023 products (WOA 2023), to remove seasonal cycle signals and avoid aliasing due to sparse historical sampling (*Swart et al.*, 2018).

https://doi.org/10.5194/essd-2026-89
Preprint. Discussion started: 23 February 2026

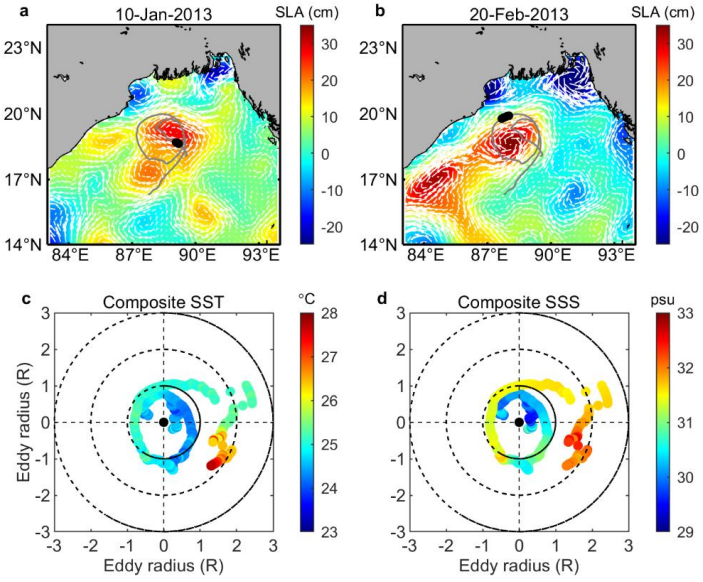

Fig.3 An example demonstrating the composite analysis of eddy effects on sea surface temperature and salinity using Argo float observations. **a-b**, Geographic distributions of sea level anomalies (colors) and geographic current anomalies (vectors) in the Bay of Bengal on January 10 2013 and February 20 2013, respectively. The gray line indicates the trajectory of the Argo float (ID: 5903744) and the black dots are its positions at the sampling day. **c-d**, Composite trajectories of the float relative to the center of the eddy. The colors are the float-estimated sea surface temperature (**c**) and sea surface salinity (**d**), respectively.

When mapping all eddy-collocated profiles in a study region to a normalized composite eddy, the scattered observations show systemically higher/lower temperature and salinity in eddy interiors than at the ambientes (Figs.4a-4c), featuring the prevailing effects of eddies on local temperature and salinity distribution. Then, by interpolating the scattered profile observations onto a standard three-dimensional grid, we can obtain the mean three-dimensional structure of eddy-induced temperature/salinity anomalies (Figs.4d-4e). Simultaneously, taking averages as a function of eddy radius can obtain the vertical section of temperature/salinity anomalies across eddy center. Mean temperature/salinity anomalies within eddies can be estimated by computing mean temperature/salinity difference between profile measurements within eddy interiors ($d < 1R$) and outside eddies (usually $d > 2R$) (*He et al.*, 2024a). The choose of profiles outside twice eddy radii as referenced background fields aims to diminish the possible influence of twisted eddy shapes, vertical eddy tilting, and the complex submesoscale processes at eddy edges (*Klein and Lapeyre*, 2009; *Li et al.*, 2022; *Siegelman et al.*, 2019).

https://doi.org/10.5194/essd-2026-89
Preprint. Discussion started: 23 February 2026

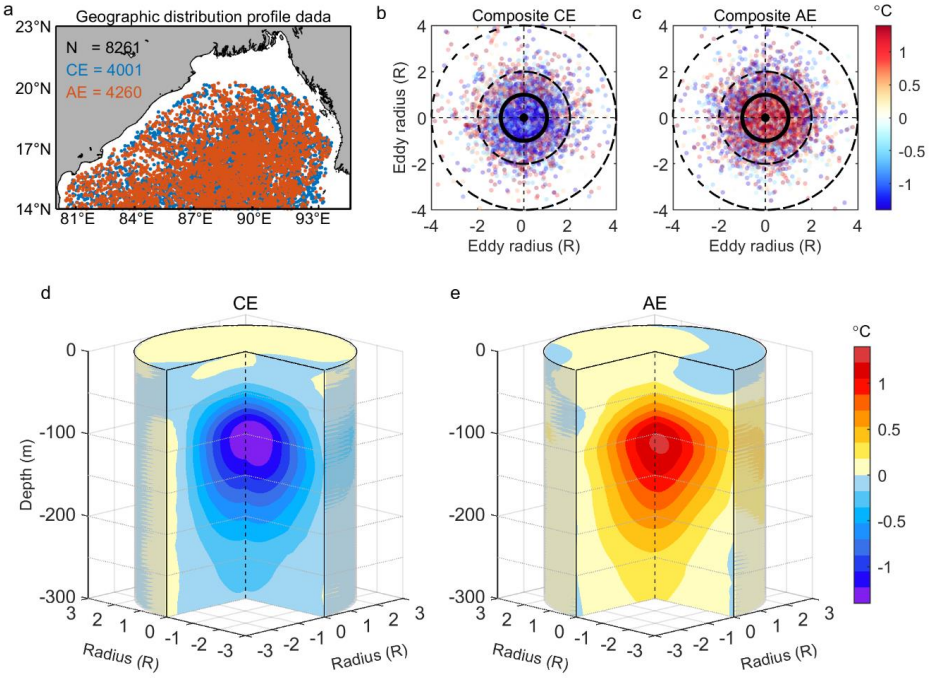

Fig.4 An example demonstrating the reconstruction of mean three-dimensional eddy temperature anomaly structures. **a**, Geographic distribution of eddy-collocated temperature profile data in the northern Bay of Bengal. The red and blue dots denote the profiles collocated with anticyclonic eddies (AE) and cyclonic eddies (CE), respectively. **b-c**, Spatial distributions of the cyclonic and anticyclonic eddy-collocated profiles (in **a**) in radius-normalized eddy-centric coordinates. The colors are the observed temperature anomalies at the depth of 100 m. **d-e**, Reconstructed mean three-dimensional eddy temperature anomaly structures by interpolating the profiles in **(b-c)** to a standard three-dimensional grid.

3. Results

3.1 Overview of the collocated data

During the period with available satellite-derived eddy data (1993–2021), 2,350,000 temperature and salinity profiles were isolated and collocated with mesoscale eddies. For each profile, the dataset provides the sampling time and location, vertical temperature and salinity distribution in the upper 1,500 m, and corresponding temperature and salinity anomalies relative to the local monthly climatology (Table 1). In addition, the relative distance and azimuth between each profile and its associated eddy are provided. The dataset also includes key properties of the matched eddy, such as eddy center location, polarity (cyclonic/anticyclonic), amplitude, radius, rotational speed, edge contour, and the trajectory number and observation number from the original eddy product (*Pegliasco et al.*,

https://doi.org/10.5194/essd-2026-89
Preprint. Discussion started: 23 February 2026

2022). The normalized distance and azimuth between each profile and the associated eddy center were also provided.

Table 1. Information of the eddy-collocated temperature and salinity profile dataset.

Variable name	Description	Variable name	Description
profile_time	Sampling date of profile data	eddy_lat	Eddy center latitude
profile_lat	Latitude of profile data	eddy_lon	Eddy center longitude
profile_lon	Latitude of profile data	eddy_iscyc	Eddy polarity (-1 for cyclonic eddy, 1 for anticyclonic eddy)
profile_instr	Observation instrument	eddy_Amp	Eddy amplitude
Temp	Temperature profile	eddy_R	Eddy radius
Sal	Salinity profile	eddy_U	Eddy rotational speed
TempA	Temperature anomaly profile	eddy_lon_contour	Longitudes of eddy edge contour
SalA	Salinity anomaly profile	eddy_lat_contour	Latitudes of eddy edge contour
MLD	Mixed layer depth	eddy_Num	Eddy trajectory number in original eddy product
Depth	Depth grids of profile data	eddy_Obs	Eddy observation number in original eddy product
Dist	Normalized distance to collocated eddy	isineddy	Is the profile located within any eddy (1 for Yes, 0 for No)
Phi	Azimuth to collocated eddy center		

The eddy-collocated profiles scattered across most regions of the global ocean, with the highest data density in the northwestern Pacific, the North Atlantic, and the northern Indian Ocean, where more than 400 profiles are available within each 2°×2° grid box (Fig.5a). Approximately 76% of the statistical grid boxes between 60°S and 60°N has more than 150 profiles. Regions with relatively lower data density are primarily located in the South Atlantic and south of the Antarctic Circumpolar Current (ACC). Nevertheless, most of these regions still contain more than 100 profiles per 2°×2° grid box, enabling the statistical analyses of eddy thermohaline imprints.

The number of the profile data is relatively small prior to the year of 2000, averaging approximately 14,000 profiles per year (Fig.5c). These profiles derived mainly from ship-based CTD observations. Following the implementation of the Argo project, the number of profile data increased rapidly after 2000 and exceeded 100,000 per year by 2008. With the additional contribution from glider observations, the accumulation of the profile data accelerated further to approximately 150,000 profiles per year after 2015, substantially enriching the observational database for investigating ocean environmental variability. It should be noted that the total number of the quality recontroled eddy-collocated profile dataset here is much smaller than the total number of raw profiles available from the WOD (>3.5 million). A major reason is the exclusion of shallow or vertically coarse sampled profiles (primarily from OSD, XBT, and APB measurements) to reduce uncertainties during the vertical interpolation of profiles to high resolution depth grids (5 m), especially in the thermocline layer with sharp temperature gradients.

https://doi.org/10.5194/essd-2026-89
Preprint. Discussion started: 23 February 2026

Open Access Earth System Science Data Discussions

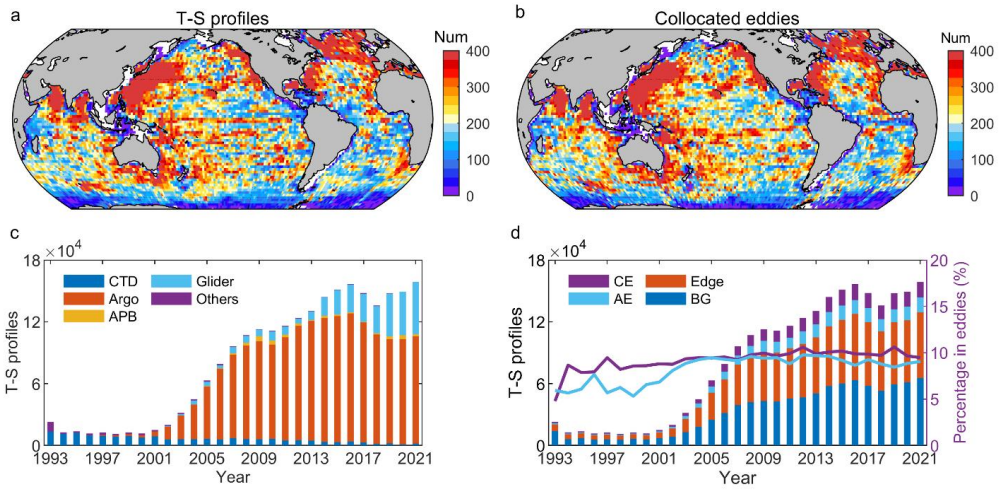

Fig.5 Spatial and temporal distributions of eddy-collocated temperature and salinity (T-S) profile data in the global ocean between 1993 and 2021. **a-b**, The number of T-S profiles (**a**) and the collocated eddies (**b**) within each 2°×2° grid box. **c**, Yearly statistics of T-S profiles from different instruments. **d**, Yearly statistics of T-S profiles within cyclonic eddies (CE, d<R), anticyclonic eddies (AE, d<R), at eddy edges (R<d<2R), and at background fields (BG, d>2R). The purple and cyan lines are the percentages of profiles within CEs and AEs, respectively.

Although the total number of profiles before the year of 2000 is much lower than that after 2000, the percentage of profiles located within mesoscale eddies remains relatively stable during all these years (nearly 10 % within cyclonic eddies and 10 % within anticyclonic eddies) (Fig.5d). Additionally, although the profiles and associated eddies exhibit high spatial heterogeneity (Fig.5b), the percentages of profiles within eddies are much more spatially uniform and highly consistent with the geographic distribution of eddy occurrence probability (Fig.6). These features suggest that the profile observations are approximately random sampled relative to mesoscale eddies. As such, the spatiotemporal inhomogeneity of the profile data may not substantially affect the analysis of eddy-induced temperature and salinity anomalies.

https://doi.org/10.5194/essd-2026-89
Preprint. Discussion started: 23 February 2026

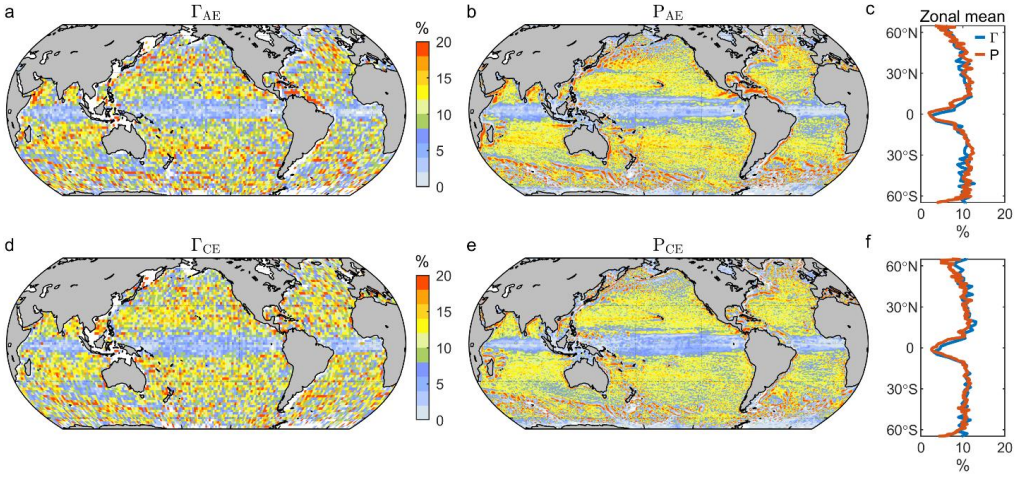

Fig.6 Consistency between the percentage of profile data within eddies and eddy occurrence probability. **a**, Geographic distribution of the percentage of profile data within anticyclonic eddies. **b**, Geographic distribution of anticyclonic eddy occurrence probability estimated from satellite-detected eddy products. **c**, Zonal averages of (**a**) and (**b**). **d-f**, The same as (**a-c**), but for cyclonic eddies.

3.2 Validation of the collocated dataset

To validate the capability of the eddy-collocated profile dataset in capturing eddy thermohaline structures, we first examined an eddy observation case that was tracked by an Argo float in the northern Bay of Bengal. The float was deployed southeast of an anticyclonic eddy at 89.5°E and 18°N on 2 January 2013 and then drifted within and around the eddy for more than one month (Figs.3a-3b). For each sampling day, the positions of the float were relocated relative to the eddy's center and mapped onto a radius-normalized eddy-centric coordinate. The resulting observations along the float trajectory show systematically lower sea surface temperature and salinity in the eddy interior compared to the surroundings (Figs.3c-3d), demonstrating that the eddy-centered composite framework is capable of revealing the thermohaline structure of the eddy.

We further extracted all eddy-collocated profiles in the northern Bay of Bengal and mapped them to an anticyclonic and cyclonic eddy-centric coordinate, respectively, based on the polarity of the collated eddies (Fig.4). The profiles are found to be approximately randomly distributed in and around the composite eddies (Figs.4b-4c), supporting the three-dimensional interpolation of the profiles to obtain three-dimensional eddy temperature anomaly structures. The results show that the core of temperature anomalies within cyclonic eddies occurs at approximately 110 m depth in eddy center, with magnitudes exceeding 1.5°C (Figs.4d-4e). The anomaly weakens with depth and becomes negligible below 300 m. The temperature anomaly structure is similar for AEs but with a slightly deeper (10 m) core and an opposite sign. These eddy patterns are consistent with *in situ* observations of eddy-associated temperature anomalies reported previously (*Sarma et al.*, 2018; *Sarma et al.*, 2020), supporting the effectiveness of the composite analysis in characterizing region mean eddy structure.

https://doi.org/10.5194/essd-2026-89
Preprint. Discussion started: 23 February 2026

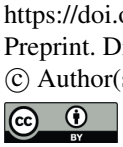

Using this collocated dataset, we reconstructed mean vertical eddy temperature anomaly structures for regions that have been investigated in previous studies, including the South China Sea (*He et al.*, 2018; *Sun et al.*, 2018), the tropical southeastern Indian Ocean (*Yang et al.*, 2015), the Kuroshio Extension (*Dong et al.*, 2017; *Sun et al.*, 2017), the southeastern Pacific Ocean (*Chaigneau et al.*, 2011), the Southern Ocean (*Frenger et al.*, 2015), and the Brazil-Malvinas Confluence (*Mason et al.*, 2017). The derived eddy structures show good agreement with the published findings (Fig.7). In addition, the use of this unified dataset and consistent methodology favors a direct interregional comparison of eddy-induced temperature anomalies. The results show that in tropical regions with strong stratification and relatively weak eddy activity (e.g., the tropical southeastern Indian Ocean and the South China Sea), eddy-induced temperature anomalies peak near the thermocline and generally do not extend deeper than 500 m. In contrast, in the southeastern Pacific, where both stratification and eddy activity are weak, eddy impacts penetrate deeper to 500 m but with relatively weak temperature anomalies (less than 1 °C). In midlatitude main current regions characterized by weak stratification and intense eddy activity, eddy-induced temperature anomalies can extend beyond 1000 m and exceed 2 °C in magnitude. Notably, despite their similar latitudes and both being western boundary currents, the vertical penetration of eddy-induced temperature anomalies in the Gulf Stream is approximately 500 m deeper than in the Kuroshio. This difference is likely related to stronger vertical stratification in the Kuroshio, which may inhibit the downward transfer of eddy energy.

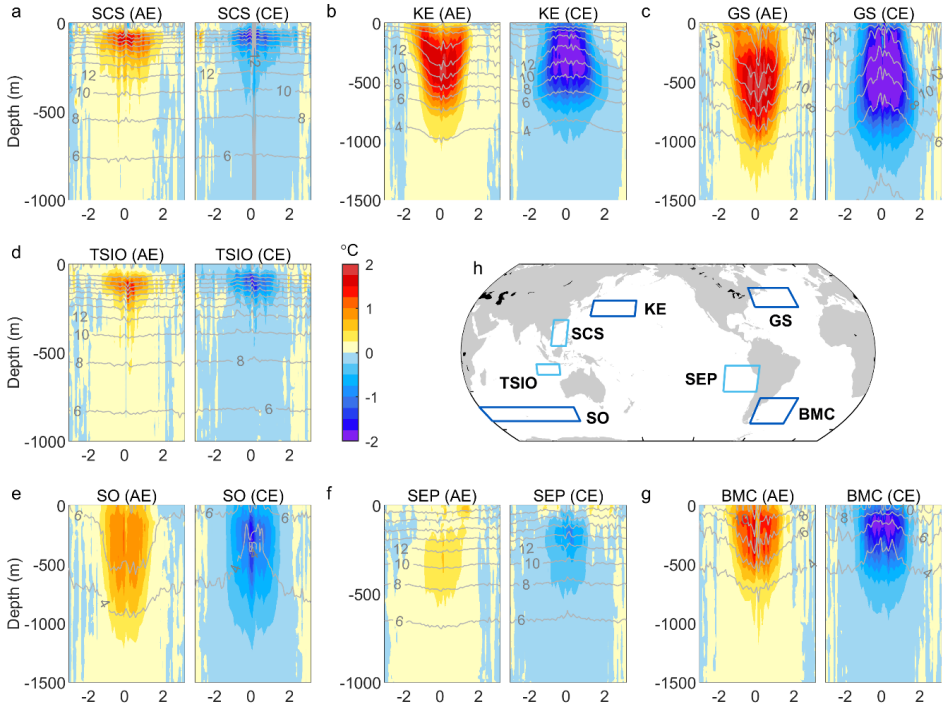

Fig.7 Composite mean eddy temperature anomaly structures in representative regions of the global

https://doi.org/10.5194/essd-2026-89
Preprint. Discussion started: 23 February 2026

ocean. **a-g**, West-east sections of mean temperature anomalies across the composite centers of anticyclonic (AE) and cyclonic (CE) eddies in the South China Sea (SCS), the Kuroshio Extension (KE), the Gulf Stream (GS), the tropical southeastern Indian Ocean (TSIO), the southeastern Pacific Ocean (SEP), the Southern Ocean (SO), and the Brazil-Malvinas Confluence (BMC). **h**, The statistical regions (boxes) of (**a-g**).

In addition to temperature, the dataset enables the construction of vertical eddy salinity anomaly structures (Fig.8). The results show that, although the tropical southeastern Indian Ocean and the South China Sea exhibit comparable temperature anomalies, the salinity anomalies in the former are substantially stronger and penetrate deeper. This contrast likely reflects the much larger subsurface vertical salinity gradient in the tropical southeastern Indian Ocean, which enhances salinity perturbations associated with vertical displacements of water masses within eddies. Another notable feature is observed in the Kuroshio Extension, the Southern Ocean, and the Brazil–Malvinas Confluence regions, where salinity anomalies within anticyclonic eddies are positive above approximately 700 m but negative below this depth, with the opposite pattern occurring in cyclonic eddies. This vertical sign reversal differs markedly from the temperature anomalies, which retain the same sign throughout the upper ocean (Fig.7). The salinity sign change is likely associated with the presence of a subsurface salinity minimum layer near this depth. Consequently, the downward displacement of this layer within AEs produces positive salinity anomalies above and negative anomalies below. In addition, horizontal advection associated with eddy migration (eddy trapping) may also contribute to the salinity anomalies. An important evidence is in the Southern Ocean, where AEs are characterized by uplifted isohalines but depressed isotherms, indicating that the eddy-induced thermohaline anomalies are not dominated by the downwelling of near-surface waters, but instead by the poleward transport of warm, saline subtropical waters across the ACC. These results not only broaden our understanding of the regional variability in eddies' impacts on temperature and salinity distributions, but also provide access to uncover the characters and mechanisms of eddies' thermohaline impacts in other regions of the global ocean.

https://doi.org/10.5194/essd-2026-89
Preprint. Discussion started: 23 February 2026

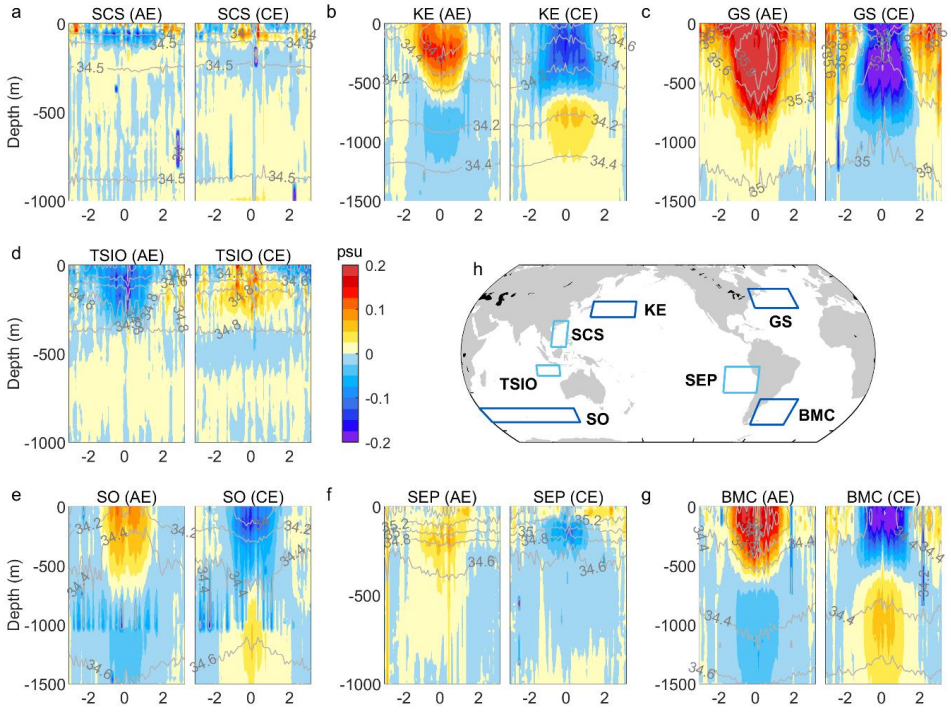

Fig.8 The same as **Fig. 7**, but for eddy salinity anomaly structures.

4. Data applications

4.1 Regional to global eddy thermohaline impacts

The strong consistency between the eddy-induced temperature anomaly structures revealed by this dataset and those reported in previous studies demonstrates that the dataset can be used to quantify the spatial heterogeneity of eddy thermohaline impacts globally. Using this dataset, we estimated eddy-associated temperature anomalies, within each 2°×2° grid, by computing the difference between the mean temperature anomalies within eddy interiors (d<1R) and that outside two eddy radii (d>2R). The results show that although AEs (CEs) are generally associated with positive (negative) temperature anomalies, their intensity vary substantially across ocean basins and depths (Fig.9).

Near the sea surface (20 m), regions of high temperature anomalies (with magnitudes >2°C) are primarily located in western boundary currents and their extensions, highly consistent with the intense eddy activities in these regions (Figs.9a-9c). In the subsurface layer (e.g., 200 m), intense temperature anomalies are also observed in subtropical gyres, with magnitudes comparable to those in western boundary currents (Figs.9d-9f). Although eddy kinetic energy in these subtropical regions is much weaker than that in the western boundary currents, the presence of thermocline layer (with strong vertical temperature gradients) allows eddy pumping to generate substantial temperature anomalies at

https://doi.org/10.5194/essd-2026-89
Preprint. Discussion started: 23 February 2026

these depths (*He et al.*, 2024a). The temperature anomalies generally weaken with depth and become negligible below 800 m in tropical and subtropical regions (Figs.9g-9i), indicating that strong stratification constrains the downward penetration of eddy effects. In contrast, western boundary current regions still exhibit temperature anomalies exceeding 1 °C at this depth, suggesting that eddy influences can extend into the deep ocean in dynamically energetic regions. Notably, the depth penetration of eddy-induced temperature anomalies in the Kuroshio Extension is markedly shallower than in the Gulf Stream. Given that eddy kinetic energy in these two regions are similar, a possible reason may be that the weaker vertical stratification in the Gulf Stream enables the deeper transfer of eddy signals.

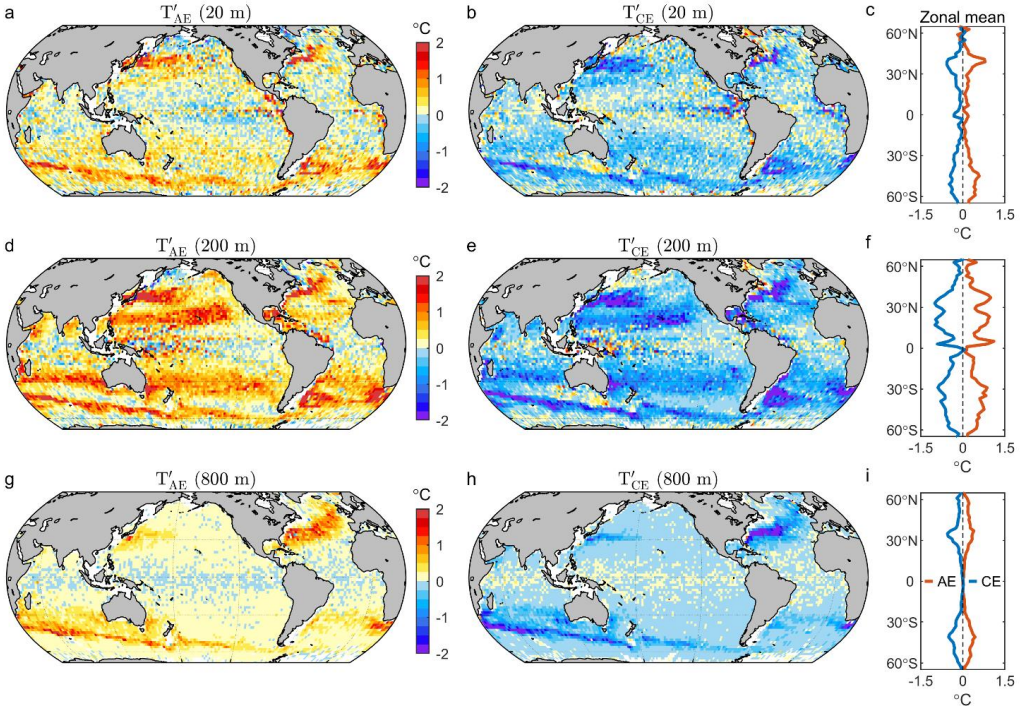

Fig.9 Spatial variability in eddy-associated temperature anomalies in the upper ocean. (a)–(h) Global distribution of mean temperature anomalies within anticyclonic eddies (AE, left), cyclonic eddies (CE, middle), and the corresponding zonal averages (right) at the depths of 20, 200, and 800 m, respectively.

The spatial patterns of eddy-induced salinity anomalies are more complex than those of temperature. Near the sea surface, anticyclonic eddies are associated with positive salinity anomalies in western boundary current regions but negative anomalies in tropical and subtropical regions, with the opposite pattern observed for cyclonic eddies (Figs.10a-10c). This latitudinal contrast arises primarily from the presence of subsurface salinity maxima layer in the tropical and subtropical oceans. In these regions, convergence and downwelling of warm and fresher near-surface water within anticyclonic eddies result in positive temperature anomalies but negative salinity anomalies (the opposite is true for

https://doi.org/10.5194/essd-2026-89
Preprint. Discussion started: 23 February 2026

364 cyclonic eddies). Below the subsurface salinity maximum layer (around 200 m), the same process
365 leads to depression of warm and salty water, thus resulting in positive temperature and salinity
366 anomalies (Figs.10d-10f). At greater depths (e.g., 800 m), a contrasting feature is the negative (positive)
367 salinity anomalies within anticyclonic (cyclonic) eddies in the North Pacific and south of the ACC,
368 opposing to the anomalies in the upper layer and at lower latitudes (Figs.10g-10i). This phenomenon
369 is likely attributable to the depress (uplift) and/or poleward transport of subsurface salinity minima
370 water at these depths.

371 Overall, eddy-associated salinity anomalies are weaker and penetrate less deeply than temperature
372 anomalies, particularly in subtropical regions (Figs.9 and 10). This difference is closely related to the
373 much weaker vertical (and horizontal) salinity gradients compared to temperature, which limits the
374 magnitude of salinity perturbations generated by eddy-induced water mass displacement. These results
375 not only demonstrate the rich regional variability in eddy-induced temperature and salinity anomalies,
376 but also provide important support for the further investigation of eddy impacts on seawater density
377 and ocean heat content, the depth penetration of eddy impacts, and the vertical displacements of water
378 mass and materials (nutrients, oxygen, and carbon) by eddies. Such analyses are essential for
379 advancing our understanding of how mesoscale eddies reshape the ocean's thermohaline structure and
380 biogeochemical environments.

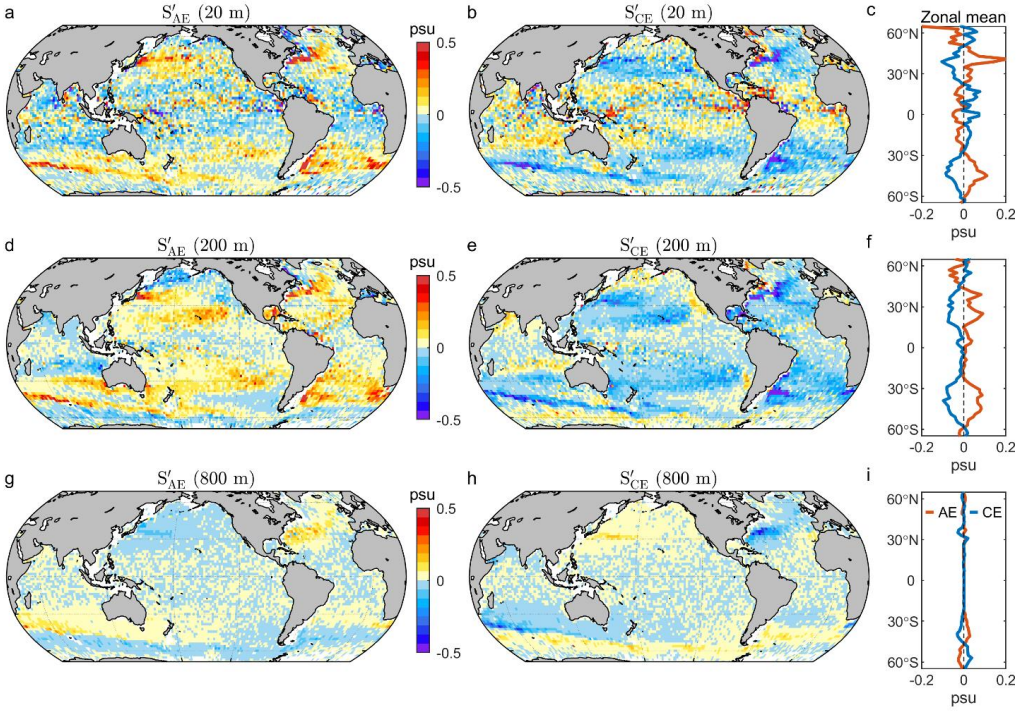

381
382 **Fig.10** The same as **Fig. 9**, but for eddy salinity anomalies.

https://doi.org/10.5194/essd-2026-89
Preprint. Discussion started: 23 February 2026

4.2 Eddy effects on mixing and stratification

Variations in temperature and salinity directly modify ocean stratification and vertical mixing. Consequently, eddy-induced thermohaline anomalies are expected to exert an apparent influence on the mixed layer depth (MLD) and upper-ocean stratification. Using the collocated eddy-collated profile dataset, we estimated mean MLD anomalies within cyclonic and anticyclonic eddies, respectively, within each 2°×2° grid box in the global ocean. At the global scale, anticyclonic eddies are generally associated with a shallower mixed layer, whereas cyclonic eddies associated with a deeper mixed layer, with typical anomaly magnitudes of 10–20 m (Fig.11). The strongest eddy-induced MLD anomalies occur in the Gulf Stream and the ACC regions, where magnitudes can exceed 50 m and locally approach 100 m. The patterns are consistent with previous statistical analyses conducted within 5°×5° grid boxes globally (*Gaube et al.*, 2019).

Compared with thermohaline anomalies, the spatial patterns of eddy-induced MLD anomalies are less regular, particularly at mid and high latitudes. This phenomenon due primarily to the strong sensitivity of MLD estimates to vertical variations in temperature and salinity (*de Boyer Montégut et al.*, 2004). As a result, MLD anomalies derived from limited samples exhibit substantially larger uncertainty than temperature or salinity anomalies. Nevertheless, this dataset enables the characterization of eddy-induced mixed-layer variability at a finer spatial resolution (2°×2°), allowing for a more detailed examination of eddy impacts in frontal regions such as the ACC and Gulf Stream. The successful mapping of eddy-induced MLD anomalies further indicates that this dataset can be applied to investigate eddy effects on thermocline depth, thermocline thickness, barrier layer thickness, and vertical stratification strength et.

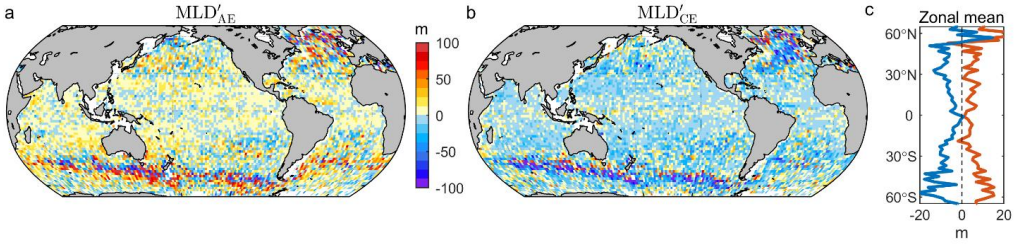

Fig.11 The same as **Fig. 9**, but for MLD anomalies.

4.3 Eddy contribution to extreme temperature events

Given the ability of eddies to generate strong temperature anomalies, they may play an important role in driving extreme temperature events (Maine Heatwaves and Cold-spells). Long-term continuous mooring observations suggest that approximately 80 % of detected extreme temperature anomalies exhibit temporal continuity (for longer than 5 days) and can therefore be identified as extreme temperature events (*He et al.*, 2024b). Accordingly, extreme temperature anomalies identified from discrete profile observations can be used as proxies for extreme temperature events. Using this dataset, we quantified the contribution of mesoscale eddies to extreme temperature events by calculating the percentage of extreme temperature anomalies occurring within eddies (Fig.12). Extreme high (low)

https://doi.org/10.5194/essd-2026-89
Preprint. Discussion started: 23 February 2026

temperature anomalies were identified as temperature anomalies exceeding 95th (below 5th) percentile climatology.

Given that anticyclonic (cyclonic) eddies are generally associated positive (negative) temperature anomalies, they are more likely to induce extreme high (low) temperature events. Thus, we focused mainly on the percentages of extreme high temperature anomalies occurred within anticyclonic eddies and extreme low temperature anomalies occurred within cyclonic eddies. At the global scale, this fraction is typically around 10% near the surface, except in the ACC region (up to 30%) (Fig.12a-12c). The ratio is comparable to the overall probability of eddy occurrence, suggesting that mesoscale eddies do not substantially enhance the occurrence of surface extreme temperature events. In contrast, in the subsurface layer (e.g., 200 m), approximately half of extreme high (low) temperature events in subtropical gyres and western boundary currents occurred within anticyclonic (cyclonic) eddies (Fig.12d-12f). This pattern persists even at depths of 1000 m, indicating that mesoscale eddies are major contributors to subsurface extreme temperature events (Fig.12g-12i). These results demonstrate that the eddy-collocated profile dataset provides a valuable observational basis for assessing eddy effects on extreme temperature events and has the potential for analogous studies of extreme salinity events.

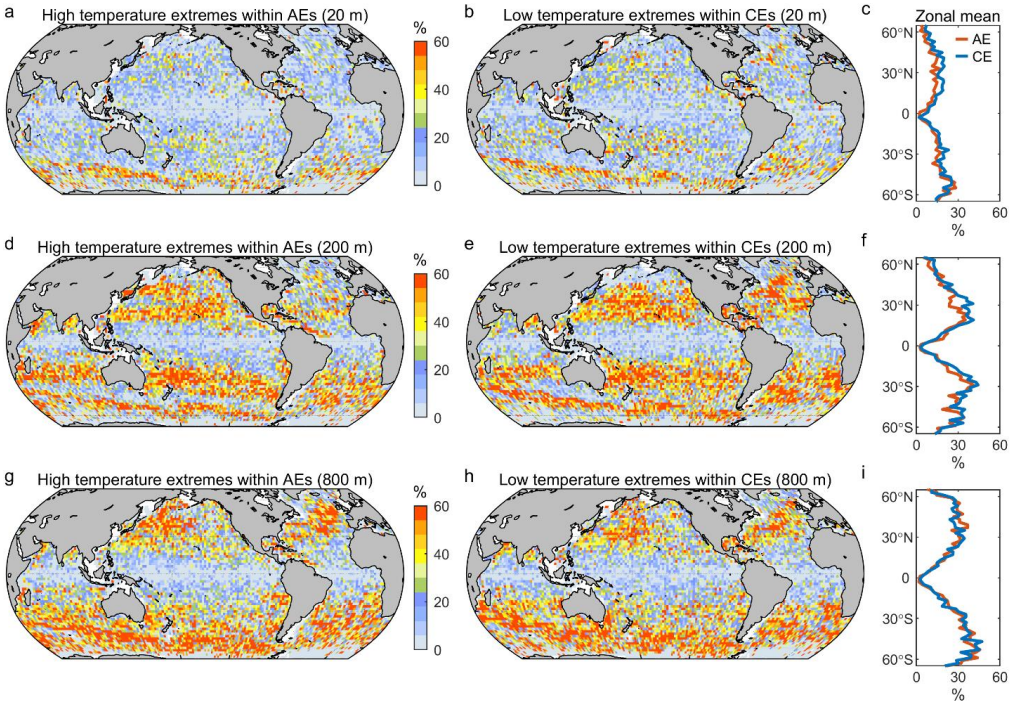

Fig.12 Spatial variability in eddy contribution to extreme temperature events in the upper ocean. (a)–(h) Global distribution of the percentages of extreme high temperature anomalies occurred within anticyclonic eddies (AE, left), extreme low temperature anomalies occurred cyclonic eddies (CE, middle), and the corresponding zonal averages (right) at the depths of 20, 200, and 800 m, respectively.

https://doi.org/10.5194/essd-2026-89
Preprint. Discussion started: 23 February 2026

4.4 Eddy-driven heat and salt transports

The dataset enables the quantification of the vertical structure of eddy-induced temperature and salinity anomalies, for each 2°×2° grid, along with eddy occurrence probability and movement velocity. These information can be used to estimate heat and salt transports induced by eddy movements and to identify regions of efficient eddy transport. Furthermore, by interpolating the eddy-collocated profiles to a standardized three-dimensional eddy centric grid, we could obtain the three-dimensional structures of eddy-induced temperature and salinity anomalies (Fig.4), and subsequently horizontal velocity and potential vorticity fields (*He et al.*, 2018). These structures can then be used to estimate the heat, salt, and water mass transports induced by eddy stirring (rotation) (*Sun et al.*, 2019). It should be noted that the current accumulated profiles may still be insufficient to robustly reconstruct mean three-dimensional eddy structures at small spatial regions (e.g., 2°×2°). However, as the amount of in situ observations continues to increase, the accuracy and resolution of such reconstructions are expected to improve. These advances are anticipated to further refine the quantification of the role of mesoscale eddies in regional to global water mass transport, heat and salt redistributions, and polar heat balance.

5. Conclusions

Mesoscale eddies are widely documented as an essential dynamical process influencing oceanic physical and biogeochemical environments from regional to global scales. However, the scarcity of eddy-targeted observations has long limited our ability to quantify how and to what extend eddies regulate temperature and salinity redistribution, heat transport, material flux, and climate-relevant processes. By integrating 29 years (1993–2022) of globally available temperature and salinity profile observations with concurrent satellite-derived eddy information, we constructed a global eddy-collocated temperature and salinity profile dataset comprising more than 2 million profiles. For each profile, the dataset provides the vertical structure of water temperature and salinity and the corresponding anomalies relative to climatology, together with information on the nearest eddy potentially influencing the observed water column on the sampling day. The dataset covers most regions of the global ocean, with more than 150 profiles available in most 2°×2° grid boxes, enabling robust statistical analyses of regional eddy thermohaline impacts. Based on this dataset, we successfully reproduced the local eddy impacts on the vertical distribution of temperature and salinity revealed by previous studies and demonstrated that it reliably captures the pronounced spatial heterogeneity of eddy-induced thermohaline anomalies, mixed layer perturbations, and extreme temperature variability within the upper 1000 m of the global ocean. These results highlight the substantial potential of this dataset for advancing studies of mesoscale eddy influences on oceanic thermohaline structure, heat and salt transports, stratification, extreme events, and their broader implications for ocean circulation and climate change.

Data availability:

The eddy-collocated T-S profile data product described in this manuscript can be accessed on Zendo at https://doi.org/10.5281/zenodo.18590979 (He, 2026). The global historical *in situ* temperature and salinity profile data used in this study is derived from the WOD at https://www.nodc.noaa.gov/OC5/WOD/pr_wod.html. The satellite-detected eddy product is delivered by the AVISO$^+$ at https://aviso.altimetry.fr. The climatology sea water temperature data (WOA 2023) is available at https://www.ncei.noaa.gov/access/world-ocean-atlas-2023/.

https://doi.org/10.5194/essd-2026-89
Preprint. Discussion started: 23 February 2026

Acknowledgments:
This work is supported by the National Natural Science Foundation of China (NSFC) (Nos. 42522601, 42494881, 42276027, and 42276186), the Strategic Priority Research Program of the Chinese Academy of Sciences (No. XDA0370101), and the China-Sri Lanka Joint Center for Education and Research, Chinese Academy of Sciences. The data analysis is supported by the High Performance Computing Division in the South China Sea Institute of Oceanology.

Author contributions:
Q.H. and H.Z. conceived the study. Q.H. conducted the analysis and wrote the paper. Y.L., W.Z., Y.H., Z.M., P.Z., S.C., and H.Z. contributed to the interpretation of the results and the revision of the manuscript.

Competing interests: Authors declare that they have no competing interests.

6. References

Amos, C. M., R. M. Castelao, and P. M. Medeiros (2019), Offshore transport of particulate organic carbon in the California Current System by mesoscale eddies, *Nature communications*, *10*(1), 1-8, doi:10.1038/s41467-019-12783-5.

Arostegui, M. C., P. Gaube, P. A. Woodworth-Jefcoats, D. R. Kobayashi, and C. D. Braun (2022), Anticyclonic eddies aggregate pelagic predators in a subtropical gyre, *Nature*, doi:10.1038/s41586-022-05162-6.

Boyer, T. P., et al. (2016), NCEI Standard Product: World Ocean Database (WOD), *NOAA National Centers for Environmental Information. Dataset*.

Braun, C. D., et al. (2025), Pelagic sharks target long-lived, retentive anticyclonic eddies in the Northwest Atlantic Ocean, *Limnol Oceanogr*, doi:10.1002/lno.70260.

Braun, C. D., P. Gaube, T. H. Sinclair-Taylor, G. B. Skomal, and S. R. Thorrold (2019), Mesoscale eddies release pelagic sharks from thermal constraints to foraging in the ocean twilight zone, *Proceedings of the National Academy of Sciences*, 201903067.

Chaigneau, A., G. Eldin, and B. Dewitte (2009), Eddy activity in the four major upwelling systems from satellite altimetry (1992–2007), *Prog Oceanogr*, *83*(1-4), 117-123, doi:10.1016/j.pocean.2009.07.012.

Chaigneau, A., A. Gizolme, and C. Grados (2008), Mesoscale eddies off Peru in altimeter records: Identification algorithms and eddy spatio-temporal patterns, *Prog Oceanogr*, *79*(2-4), 106-119, doi:10.1016/j.pocean.2008.10.013.

Chaigneau, A., M. Le Texier, G. Eldin, C. Grados, and O. Pizarro (2011), Vertical structure of mesoscale eddies in the eastern South Pacific Ocean: A composite analysis from altimetry and Argo profiling floats, *J Geophys Res*, *116*(C11), doi:10.1029/2011jc007134.

Chelton, D. B., P. Gaube, M. G. Schlax, J. J. Early, and R. M. Samelson (2011a), The influence of nonlinear mesoscale eddies on near-surface oceanic chlorophyll, *Science*, *334*(6054), 328-332, doi:10.1126/science.1208897.

Chelton, D. B., M. G. Schlax, and R. M. Samelson (2011b), Global observations of nonlinear mesoscale eddies, *Prog Oceanogr*, *91*(2), 167-216, doi:10.1016/j.pocean.2011.01.002.

de Boyer Montégut, C., G. Madec, A. S. Fischer, A. Lazar, and D. Iudicone (2004), Mixed layer depth

https://doi.org/10.5194/essd-2026-89
Preprint. Discussion started: 23 February 2026

519 over the global ocean: An examination of profile data and a profile-based climatology, *J Geophys*
520 *Res*, *109*, C12003, doi:10.1029/2004jc002378.
521 de Marez, C., P. L'Hégaret, M. Morvan, and X. Carton (2019), On the 3D structure of eddies in the
522 Arabian Sea, *Deep Sea Research Part I: Oceanographic Research Papers*, *150*,
523 doi:10.1016/j.dsr.2019.06.003.
524 Delcroix, T., A. Chaigneau, D. Soviadan, J. Boutin, and C. Pegliasco (2019), Eddy-Induced Salinity
525 Changes in the Tropical Pacific, *J Geophys Res Oceans*, *124*(1), 374-389,
526 doi:10.1029/2018jc014394.
527 Dong, C., J. C. McWilliams, Y. Liu, and D. Chen (2014), Global heat and salt transports by eddy
528 movement, *Nature communications*, *5*(1), 1-6, doi:10.1038/ncomms4294.
529 Dong, D., P. Brandt, P. Chang, F. Schütte, X. Yang, J. Yan, and J. Zeng (2017), Mesoscale eddies in
530 the northwestern Pacific Ocean: Three-dimensional eddy structures and heat/salt transports, *J*
531 *Geophys Res Oceans*, *122*(12), 9795-9813.
532 Ferrari, R., and C. Wunsch (2009), Ocean Circulation Kinetic Energy: Reservoirs, Sources, and Sinks,
533 *Annu Rev Fluid Mech*, *41*(1), 253-282, doi:10.1146/annurev.fluid.40.111406.102139.
534 Frenger, I., N. Gruber, R. Knutti, and M. Münnich (2013), Imprint of Southern Ocean eddies on winds,
535 clouds and rainfall, *Nature Geoscience*, *6*(8), 608-612, doi:10.1038/ngeo1863.
536 Frenger, I., M. Münnich, and N. Gruber (2018), Imprint of Southern Ocean mesoscale eddies on
537 chlorophyll, *Biogeosciences*, *15*(15), 4781-4798, doi:10.5194/bg-15-4781-2018.
538 Frenger, I., M. Münnich, N. Gruber, and R. Knutti (2015), Southern Ocean eddy phenomenology, *J*
539 *Geophys Res Oceans*, *120*(7413-7449), doi:10.1002/2015JC011047.
540 Gaube, P., D. B. Chelton, P. G. Strutton, and M. J. Behrenfeld (2013), Satellite observations of
541 chlorophyll, phytoplankton biomass, and Ekman pumping in nonlinear mesoscale eddies, *J*
542 *Geophys Res Oceans*, *118*(12), 6349-6370, doi:10.1002/2013JC009027.
543 Gaube, P., D. J. McGillicuddy, and A. J. Moulin (2019), Mesoscale Eddies Modulate Mixed Layer
544 Depth Globally, *Geophys Res Lett*, *46*(3), 1505-1512, doi:10.1029/2018gl080006.
545 Gaube, P., D. J. McGillicuddy, D. B. Chelton, M. J. Behrenfeld, and P. G. Strutton (2014), Regional
546 variations in the influence of mesoscale eddies on near-surface chlorophyll, *J Geophys Res Oceans*,
547 *119*, 8195-8220, doi:10.1002/2014JC010111.
548 Gulakaram, V. S., N. K. Vissa, and P. K. Bhaskaran (2020), Characteristics and vertical structure of
549 oceanic mesoscale eddies in the Bay of Bengal, *Dynam Atmos Oceans*, *89*,
550 doi:10.1016/j.dynatmoce.2020.101131.
551 Guo, Y., and M. L. Timmermans (2024), The Role of Ocean Mesoscale Variability in Air-Sea CO2
552 Exchange: A Global Perspective, *Geophys Res Lett*, *51*(10), doi:10.1029/2024gl108373.
553 Hasson, A., J. T. Farrar, J. Boutin, F. Bingham, and T. Lee (2019), Intraseasonal Variability of Surface
554 Salinity in the Eastern Tropical Pacific Associated With Mesoscale Eddies, *J Geophys Res Oceans*,
555 *124*(4), 2861-2875, doi:10.1029/2018jc014175.
556 He, Q. (2026). A global eddy-collocated temperature and salinity profile dataset (V1.0), [Data set],
557 Zenodo, https://doi.org/10.5281/zenodo.18590979.
558 He, Q., D. Mo, W. Zhan, S. Cai, S. Tang, G. Zha, and H. Zhan (2024a), Thermal Imprints of Mesoscale
559 Eddies in the Global Ocean, *J Phys Oceanogr*, *54*(9), 1991-2009, doi:10.1175/jpo-d-23-0226.1.
560 He, Q., H. Zhan, and S. Cai (2020), Anticyclonic eddies enhance the winter barrier layer and surface
561 cooling in the Bay of Bengal, *J Geophys Res Oceans*, *125*(10), e2020JC016524,
562 doi:10.1029/2020JC016524.

https://doi.org/10.5194/essd-2026-89
Preprint. Discussion started: 23 February 2026

He, Q., H. Zhan, S. Cai, Y. He, G. Huang, and W. Zhan (2018), A new assessment of mesoscale eddies in the South China Sea: Surface features, three-dimensional structures and thermohaline transports *J Geophys Res Oceans*, *123*(7), 4906-4929, doi:10.1029/2018jc014054.

He, Q., H. Zhan, S. Cai, and W. Zhan (2021), Eddy-Induced Near-Surface Chlorophyll Anomalies in the Subtropical Gyres: Biomass or Physiology?, *Geophys Res Lett*, *48*(7), e2020GL091975, doi:10.1029/2020gl091975.

He, Q., H. Zhan, Y. Shuai, S. Cai, Q. P. Li, G. Huang, and J. Li (2017), Phytoplankton bloom triggered by an anticyclonic eddy: The combined effect of eddy-Ekman pumping and winter mixing, *J Geophys Res Oceans*, *122*(6), 4886-4901, doi:10.1002/2017JC012763.

He, Q., W. Zhan, M. Feng, Y. Gong, S. Cai, and H. Zhan (2024b), Common occurrences of subsurface heatwaves and cold spells in ocean eddies, *Nature*, *634*, 1111–1117, doi:10.1038/s41586-024-08051-2.

Jan, S., V. Mensah, M. Andres, M.-H. Chang, and Y. J. Yang (2017), Eddy-Kuroshio Interactions: Local and Remote Effects, *J Geophys Res Oceans*, *122*(12), 9744-9764, doi:10.1002/2017jc013476.

Jing, Z., et al. (2020), Maintenance of mid-latitude oceanic fronts by mesoscale eddies, *Science Advances*, *6*(31), eaba7880, doi:10.1126/sciadv.aba7880.

Klein, P., and G. Lapeyre (2009), The oceanic vertical pump induced by mesoscale and submesoscale turbulence, *Annual review of marine science*, *1*, 351-375, doi:10.1146/annurev.marine.010908.163704.

Laxenaire, R., S. Speich, and A. Stegner (2019), Evolution of the thermohaline structure of one Agulhas ring reconstructed from satellite altimetry and Argo floats, *J Geophys Res Oceans*, *124*(12), 8969-9003, doi:10.1029/2018JC014426.

Li, H., F. Xu, and G. Wang (2022), Global Mapping of Mesoscale Eddy Vertical Tilt, *J Geophys Res Oceans*, *127*(11), doi:10.1029/2022jc019131.

Lin, X., C. Dong, D. Chen, Y. Liu, J. Yang, B. Zou, and Y. Guan (2015), Three-dimensional properties of mesoscale eddies in the South China Sea based on eddy-resolving model output, *Deep-sea Res Pt I*, *99*, 46-64, doi:10.1016/j.dsr.2015.01.007.

Liu, T., R. Abernathey, A. Sinha, and D. Chen (2019), Quantifying Eulerian Eddy Leakiness in an Idealized Model, *J Geophys Res Oceans*, *124*(12), 8869-8886, doi:10.1029/2019jc015576.

Lv, M., F. Wang, Y. Li, Z. Zhang, and Y. Zhu (2022), Structure of Sea Surface Temperature Anomaly Induced by Mesoscale Eddies in the North Pacific Ocean, *J Geophys Res Oceans*, *127*(3), doi:10.1029/2021jc017581.

Mason, E., A. Pascual, P. Gaube, S. Ruiz, J. L. Pelegrí, and A. Delepoulle (2017), Subregional characterization of mesoscale eddies across the Brazil-Malvinas Confluence, *J Geophys Res Oceans*, *122*(4), 3329-3357, doi:10.1002/2016JC012611.

McGillicuddy, D. J., Jr. (2016), Mechanisms of physical-biological-biogeochemical interaction at the oceanic mesoscale, *Annual review of marine science*, *8*, 125-159, doi:10.1146/annurev-marine-010814-015606.

Moreau, S., A. D. Penna, J. Llort, R. Patel, C. Langlais, P. W. Boyd, R. J. Matear, H. E. Phillips, T. W. Trull, and B. Tilbrook (2017), Eddy-induced carbon transport across the Antarctic Circumpolar Current, *Global Biogeochem Cy*, doi:10.1002/2017GB005669.

Ni, Q., X. Zhai, X. Jiang, and D. Chen (2021), Abundant Cold Anticyclonic Eddies and Warm Cyclonic Eddies in the Global Ocean, *J Phys Oceanogr*, *51*(9), 2793-2806, doi:10.1175/jpo-d-21-0010.1.

Omand, M. M., E. A. D'Asaro, C. M. Lee, M. J. Perry, N. Briggs, I. Cetinic, and A. Mahadevan (2015),

https://doi.org/10.5194/essd-2026-89
Preprint. Discussion started: 23 February 2026

Eddy-driven subduction exports particulate organic carbon from the spring bloom, *Science*, *348*(6231), 222-225, doi:10.1126/science.1260062.

Pegliasco, C., A. Delepoulle, E. Mason, R. Morrow, Y. Faugère, and G. Dibarboure (2022), META3.1exp: a new global mesoscale eddy trajectory atlas derived from altimetry, *Earth System Science Data*, *14*(3), 1087-1107, doi:10.5194/essd-14-1087-2022.

Riser, S. C., et al. (2016), Fifteen years of ocean observations with the global Argo array, *Nature Climate Change*, *6*(2), 145-153, doi:10.1038/nclimate2872.

Samelson, R. M., M. G. Schlax, and D. B. Chelton (2014), Randomness, symmetry, and scaling of mesoscale eddy life cycles, *J Phys Oceanogr*, *44*(3), 1012-1029, doi:10.1175/jpo-d-13-0161.1.

Sarma, V., L. Jagadeesan, H. Dalabehera, D. Rao, G. Kumar, D. Durgadevi, K. Yadav, S. Behera, and M. Priya (2018), Role of eddies on intensity of oxygen minimum zone in the Bay of Bengal, *Cont Shelf Res*, *168*, 48-53, doi:https://doi.org/10.1016/j.csr.2018.09.008.

Sarma, V. V. S. S., M. Chopra, D. N. Rao, M. M. R. Priya, G. R. Rajula, D. S. R. Lakshmi, and V. D. Rao (2020), Role of eddies on controlling total and size-fractionated primary production in the Bay of Bengal, *Cont Shelf Res*, *204*, 104186, doi:10.1016/j.csr.2020.104186.

Schütte, F., J. Karstensen, G. Krahmann, H. Hauss, B. Fiedler, P. Brandt, M. Visbeck, and A. Körtzinger (2016), Characterization of "dead-zone" eddies in the eastern tropical North Atlantic, *Biogeosciences*, *13*(20), 5865-5881, doi:10.5194/bg-13-5865-2016.

Siegelman, L., P. Klein, P. Rivière, A. F. Thompson, H. S. Torres, M. Flexas, and D. Menemenlis (2019), Enhanced upward heat transport at deep submesoscale ocean fronts, *Nature Geoscience*, *13*(1), 50-55, doi:10.1038/s41561-019-0489-1.

Sun, B., C. Liu, and F. Wang (2019), Global meridional eddy heat transport inferred from Argo and altimetry observations, *Scientific reports*, *9*(1), 1345, doi:10.1038/s41598-018-38069-2.

Sun, W., C. Dong, W. Tan, Y. Liu, Y. He, and J. Wang (2018), Vertical Structure Anomalies of Oceanic Eddies and Eddy-Induced Transports in the South China Sea, *Remote Sensing*, *10*(5), 795, doi:10.3390/rs10050795.

Sun, W., C. Dong, R. Wang, Y. Liu, and K. Yu (2017), Vertical structure anomalies of oceanic eddies in the Kuroshio Extension region, *J Geophys Res Oceans*, *122*(2), 1476-1496, doi:10.1002/2016jc012226.

Swart, N. C., S. T. Gille, J. C. Fyfe, and N. P. Gillett (2018), Recent Southern Ocean warming and freshening driven by greenhouse gas emissions and ozone depletion, *Nature Geoscience*, *11*(11), 836-841, doi:10.1038/s41561-018-0226-1.

Trott, C. B., B. Subrahmanyam, A. Chaigneau, and H. L. Roman-Stork (2019), Eddy-Induced Temperature and Salinity Variability in the Arabian Sea, *Geophys Res Lett*, *46*(5), 2734-2742, doi:https://doi.org/10.1029/2018GL081605.

Villas Bôas, A. B., O. T. Sato, A. Chaigneau, and G. P. Castelão (2015), The signature of mesoscale eddies on the air-sea turbulent heat fluxes in the South Atlantic Ocean, *Geophys Res Lett*, *42*(6), 1856-1862, doi:10.1002/2015gl063105.

Wei, L., and C. Wang (2025), Unraveling trapping and stirring contributions to eddy-induced heat transport in the Agulhas leakage region, *Limnol Oceanogr*, doi:10.1002/lno.70266.

Xu, L., P. Li, S. P. Xie, Q. Liu, C. Liu, and W. Gao (2016), Observing mesoscale eddy effects on mode-water subduction and transport in the North Pacific, *Nature communications*, *7*, 10505, doi:10.1038/ncomms10505.

Yang, G., F. Wang, Y. Li, and P. Lin (2013), Mesoscale eddies in the northwestern subtropical Pacific

https://doi.org/10.5194/essd-2026-89
Preprint. Discussion started: 23 February 2026

651 Ocean: Statistical characteristics and three-dimensional structures, *J Geophys Res Oceans*, *118*(4),
652 1906-1925, doi:10.1002/jgrc.20164.
653 Yang, G., W. Yu, Y. Yuan, X. Zhao, F. Wang, G. Chen, L. Liu, and Y. Duan (2015), Characteristics,
654 vertical structures, and heat/salt transports of mesoscale eddies in the southeastern tropical Indian
655 Ocean, *J Geophys Res Oceans*, *120*(10), 6733-6750, doi:10.1002/2015JC011130.
656 Zhan, W., Q. He, Y. Zhang, and H. Zhan (2023), Anticyclone Eddies Favor the Genesis of Off-Season
657 Tropical Cyclone in the Western North Pacific, *Journal of Geophysical Research: Atmospheres*,
658 *128*(1), doi:10.1029/2022jd036945.
659 Zhang, W.-Z., Q. Ni, and H. Xue (2018), Composite eddy structures on both sides of the Luzon Strait
660 and influence factors, *Ocean Dynamics*, doi:10.1007/s10236-018-1207-z.
661 Zhang, Z., W. Wang, and B. Qiu (2014), Oceanic mass transport by mesoscale eddies, *Science*,
662 *345*(6194), 322-324, doi:10.1126/science.1252418.
663 Zhang, Z., Y. Zhang, W. Wang, and R. X. Huang (2013), Universal structure of mesoscale eddies in
664 the ocean, *Geophys Res Lett*, *40*(14), 3677-3681, doi:10.1002/grl.50736.
665